

MOF-derived CoS_x as a bifunctional electrocatalyst for efficient sulfide oxidation and coupled ammonia synthesis

Kwangyeol Baek¹‡, Tianlei Li²‡, Changsoo Lee^{1,3}, Wenzhen Li^{2*}, Kwiyong Kim^{1,3*}

Affiliation

¹ Department of Civil, Urban, Earth, and Environmental Engineering, Ulsan National Institute of Science and Technology (UNIST), 50 UNIST-gil, Eonyang-eup, Ulju-gun, Ulsan, 44919, Republic of Korea

² Department of Chemical and Biological Engineering, Iowa State University, 618 Bissell Road, Ames, IA 50011, USA

³ Graduate School of Carbon Neutrality, Ulsan National Institute of Science and Technology (UNIST), 50 UNIST-gil, Eonyang-eup, Ulju-gun, Ulsan, 44919, Republic of Korea

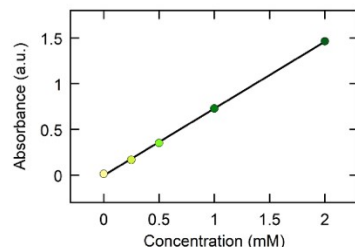
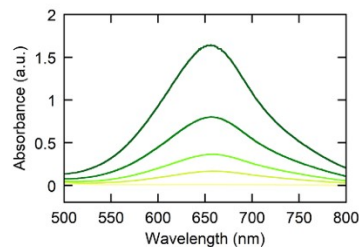
‡ K.B. and T.L contributed equally.

Corresponding author:

Wenzhen Li (wzli@iastate.edu)

Kwiyoung Kim (kwiyoungk@unist.ac.kr)

a Ammonium quantification – Indophenol reagent



b Nitrite quantification – Griess reagent

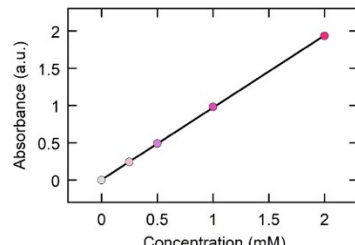
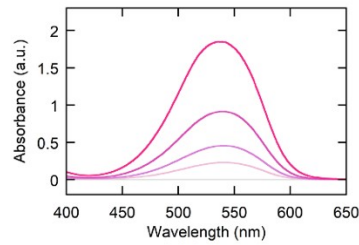


Figure S1. Calibration curves of (a) NH_4^+ and (b) NO_2^- using UV-vis spectrophotometry.

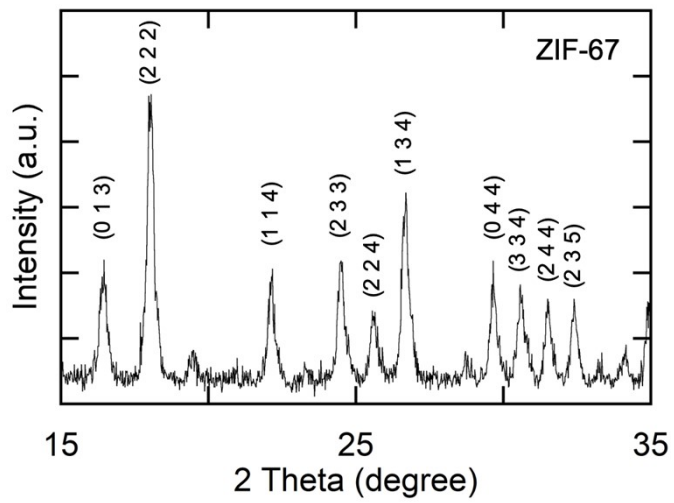


Figure S2. A XRD pattern of the synthesized ZIF-67.

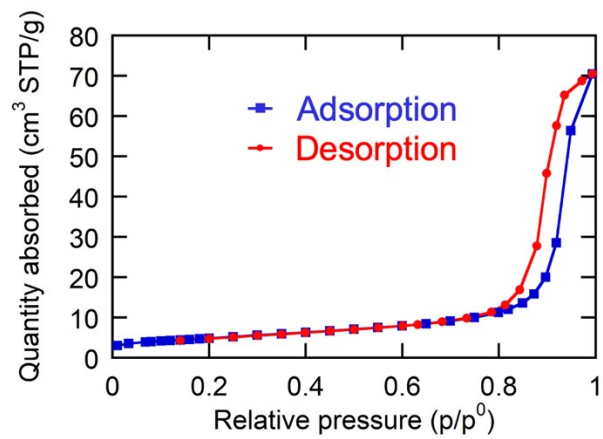
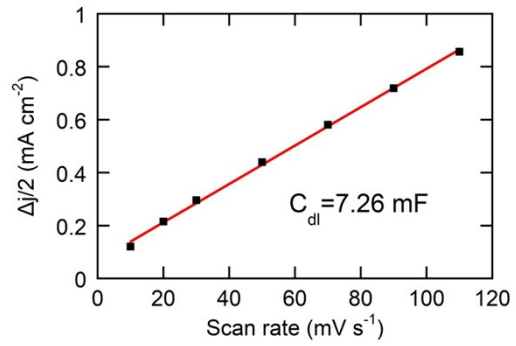
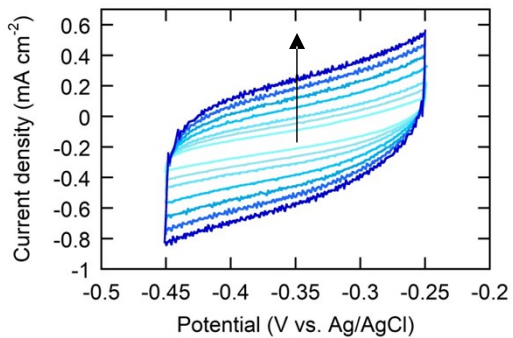


Figure S3. Nitrogen adsorption–desorption isotherm of MOF-derived CoS_x.

a MOF-derived CoS_x



b Commercial cobalt sulfide – from Sigma-Aldrich

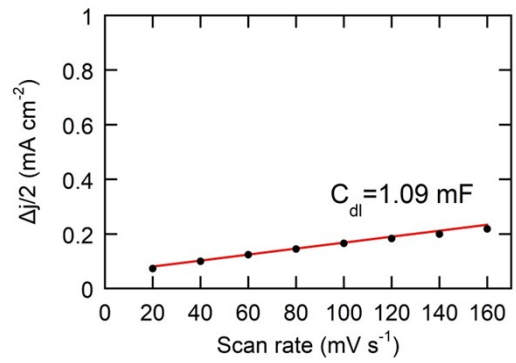
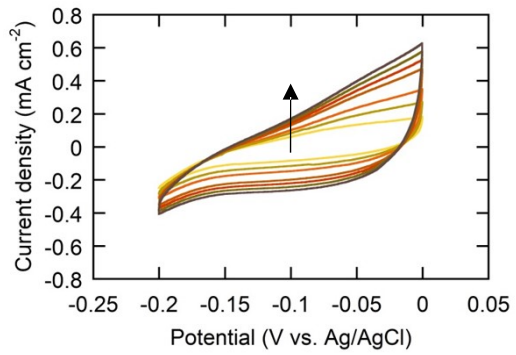


Figure S4. Electrochemical surface area estimated by cyclic voltammetry for (a) MOF-derived CoS_x and (b) commercial cobalt sulfide.

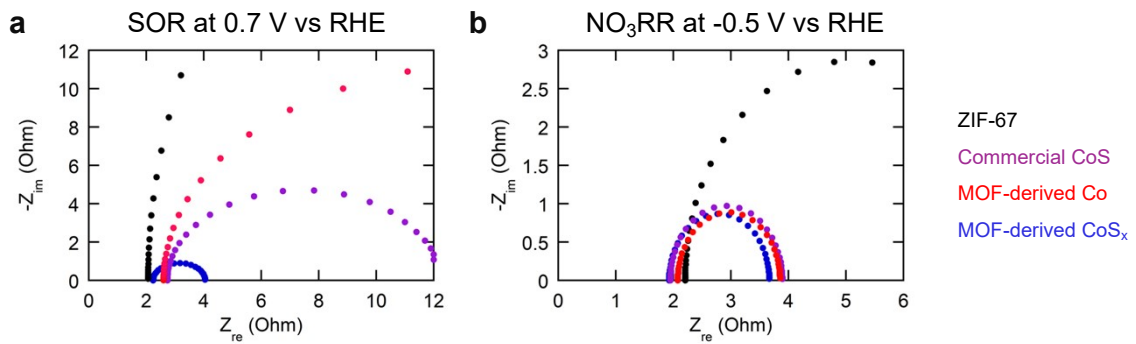


Figure S5. (a) Nyquist plots of various catalysts recorded at 0.7 V vs RHE in 1 M NaOH containing 1 M Na₂S for SOR. (b) Nyquist plots of various catalysts recorded at -0.5 V vs RHE in 1 M NaOH containing 0.1 M NaNO₃ for NO₃RR.

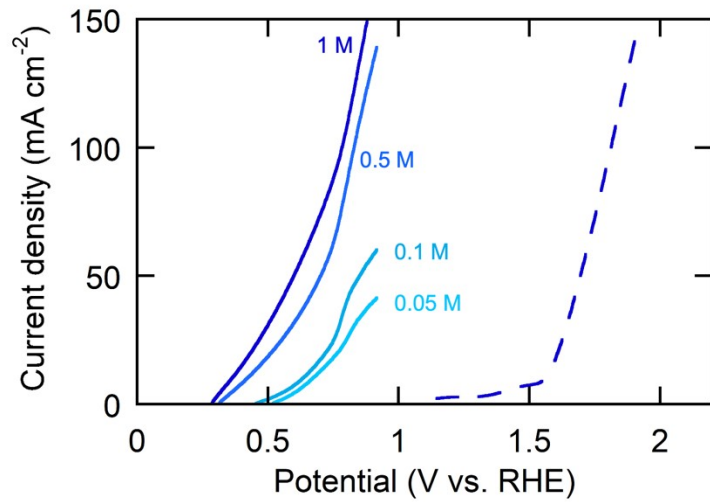


Figure S6. LSV curves of MOF-derived CoS_x for SOR at different initial Na₂S concentrations in 1 M NaOH. The dashed line indicates LSV for OER.

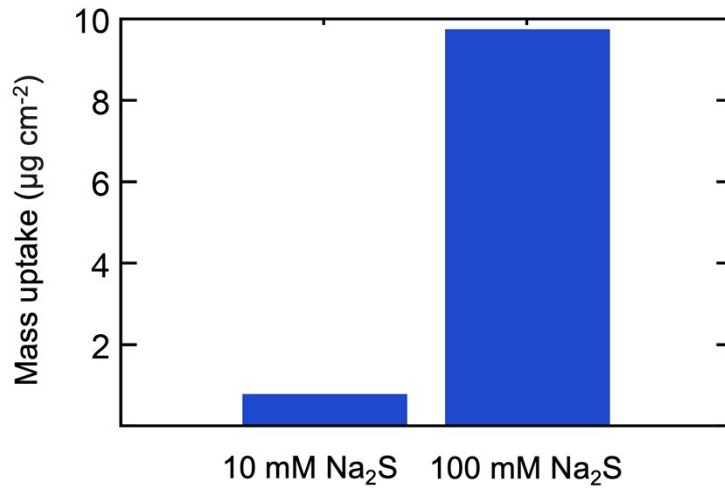


Figure S7. Uptake of sulfide ion by MOF-derived CoS_x measured using EQCM. The mass loading of the catalyst on quartz crystals was 1 mg.

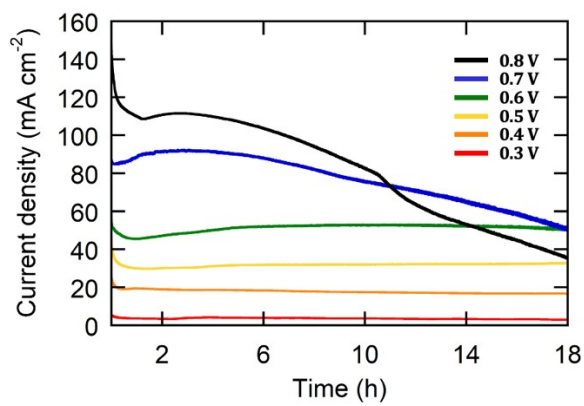


Figure S8. *Current density–time* curves during chronoamperometric operation for SOR at different applied potentials for 18 h. The anolyte was 1 M Na₂S + 1 M NaOH.

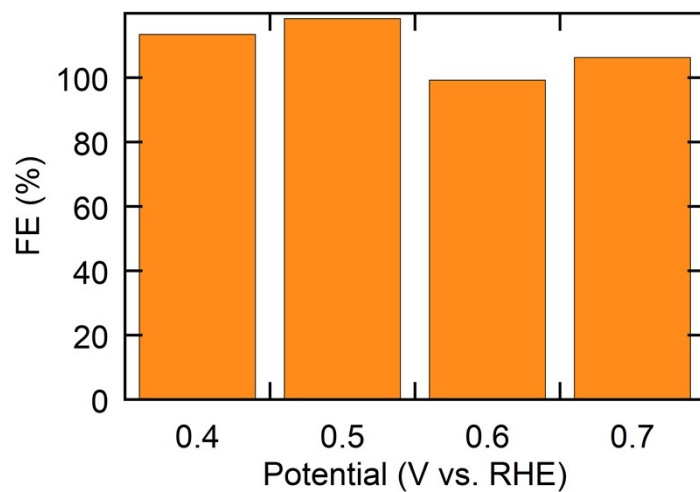


Figure S9. FE of 2e- SOR at different applied potentials. The calculations were based on *i-t* curve shown in **Figure S8**.

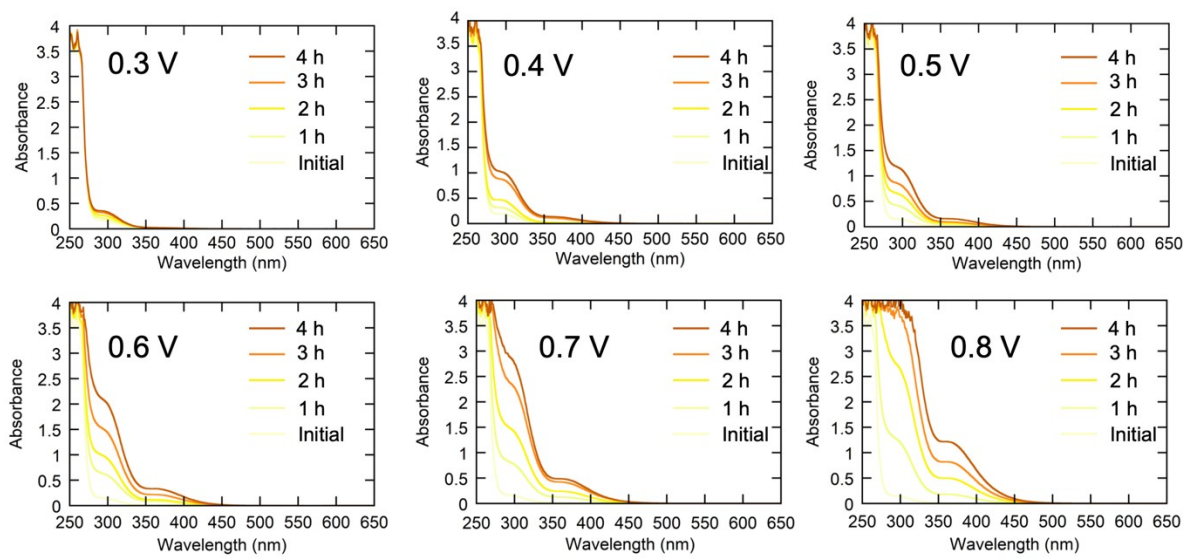


Figure S10. UV-vis spectra of the anolyte diluted 25 times at various applied potentials for SOR.

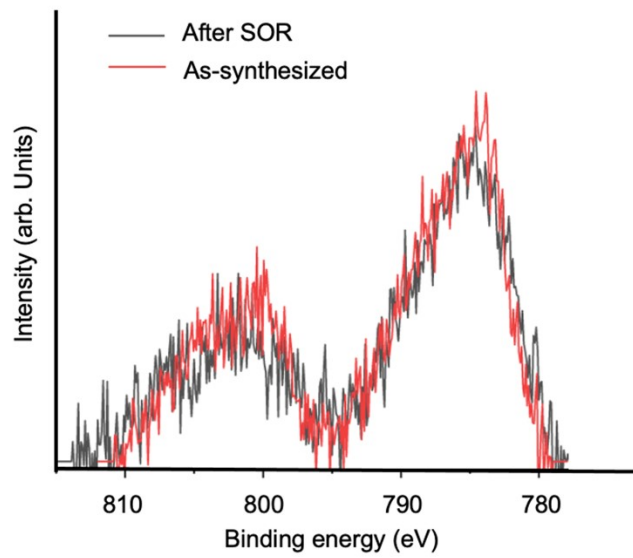


Figure S11. XPS Co 2p spectra of as-synthesized catalyst and MOF-derived CoSx after 150 h durability test at 0.8 V vs RHE.

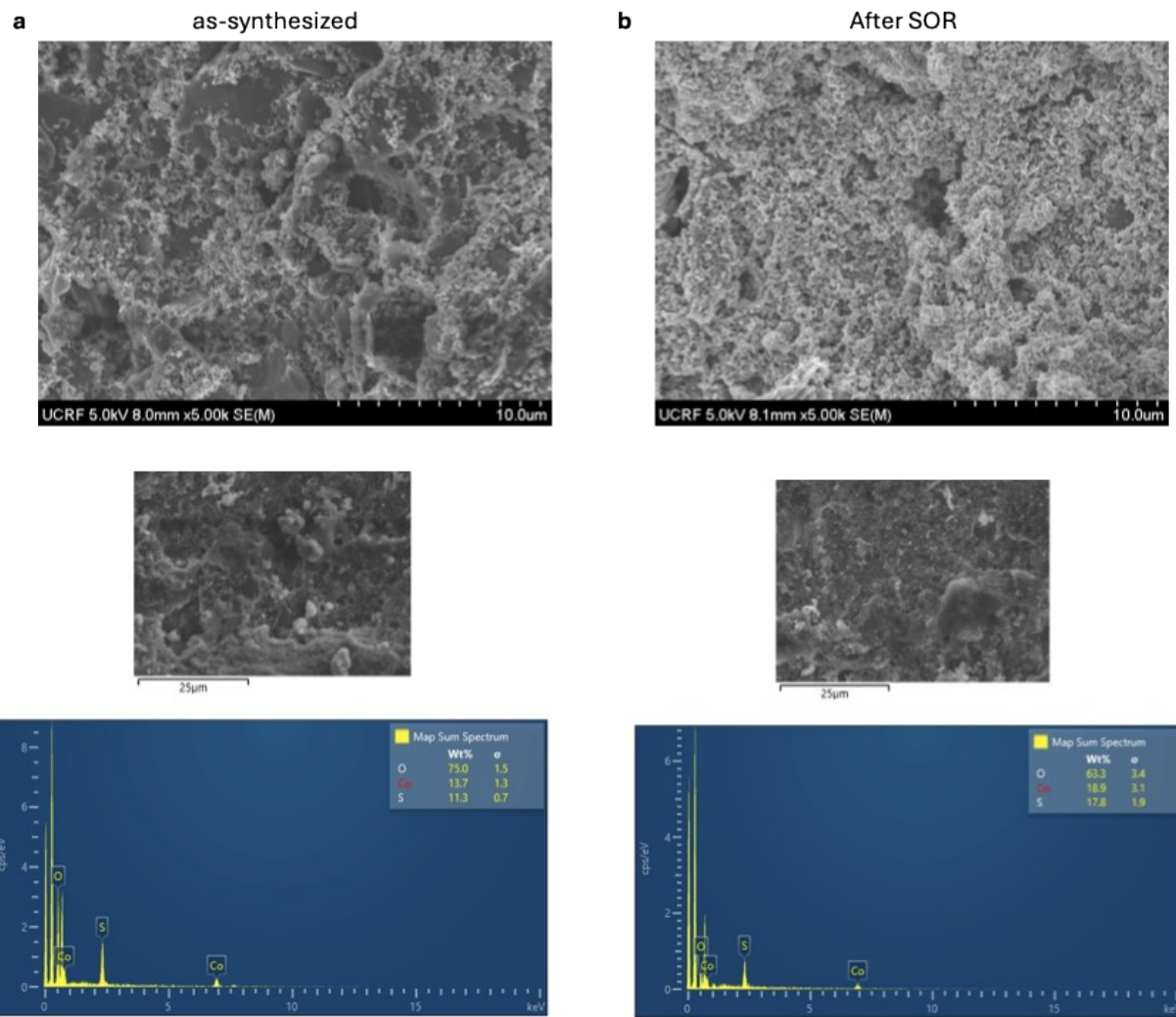


Figure S12. SEM and EDS analysis of MOF-derived CoSx (a) before and (b) after 150 h

durability test.

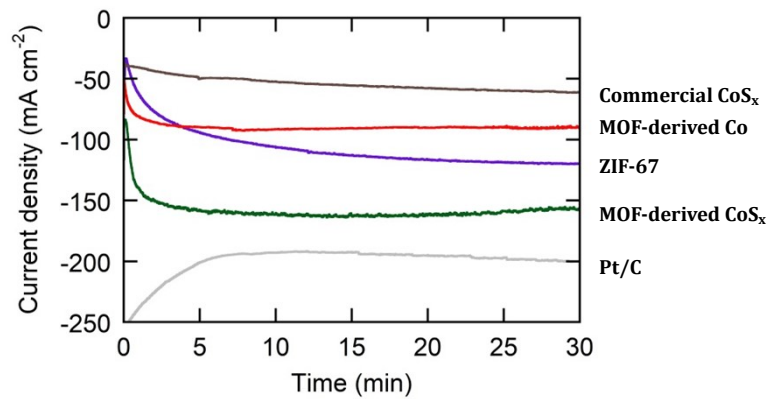


Figure S13. i - t curve during NO_3RR at -0.5 V vs RHE using various electrode materials.

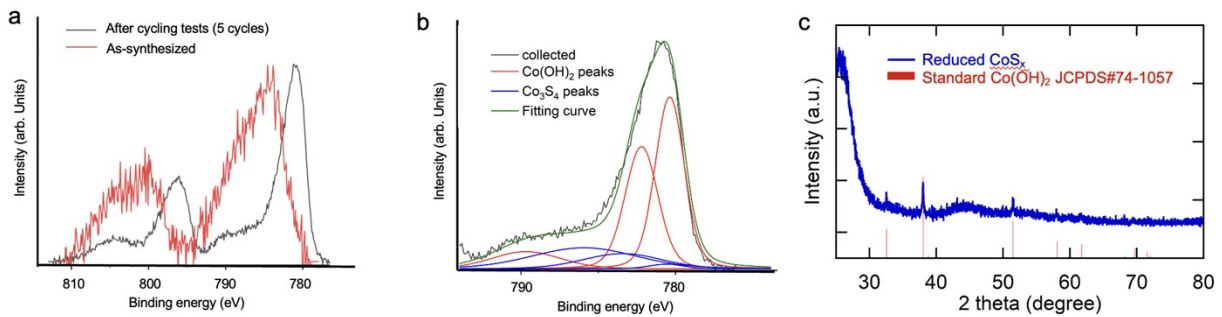


Figure S14. (a) XPS Co 2p spectra of the as-synthesized catalyst (red) and MOF-derived CoS_x after five cycles of testing at -0.5 V vs. RHE (black). (b) Fitted curves of the spent catalyst from (a). (c) XRD pattern of the spent MOF-derived CoS_x after electrochemical reduction.

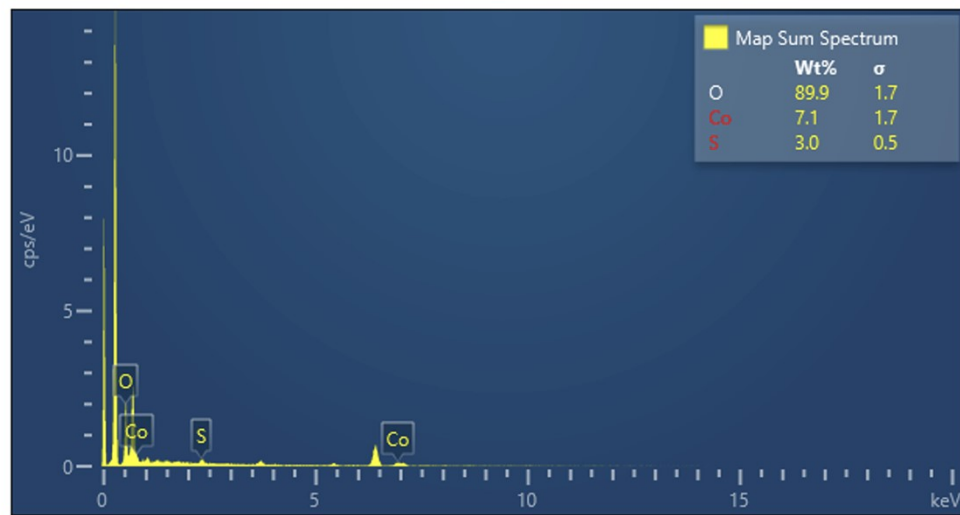
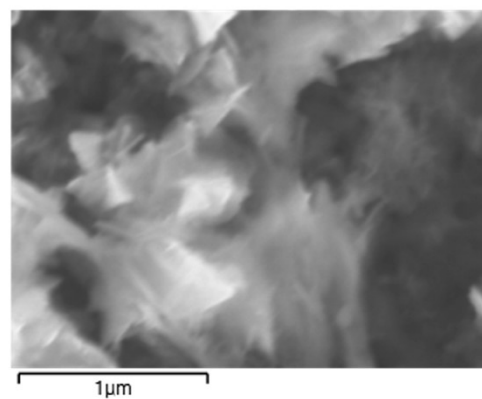
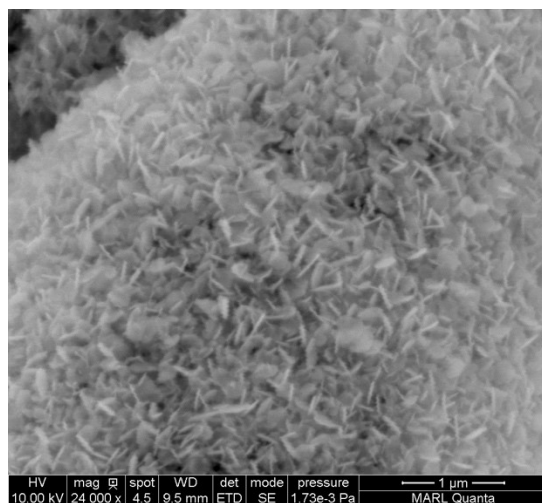


Figure S15. A SEM image and EDS analysis result of MOF-derived CoS_x after 5 cycles of testing at -0.5 V vs. RHE.

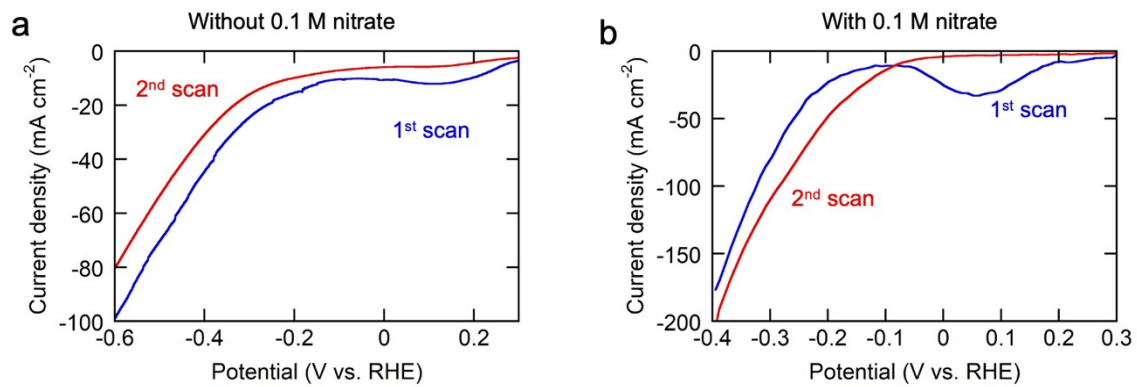


Figure S16. LSV curves of MOF-derived CoS_x (a) without nitrate and (b) with 0.1 M nitrate in background 1 M NaOH.

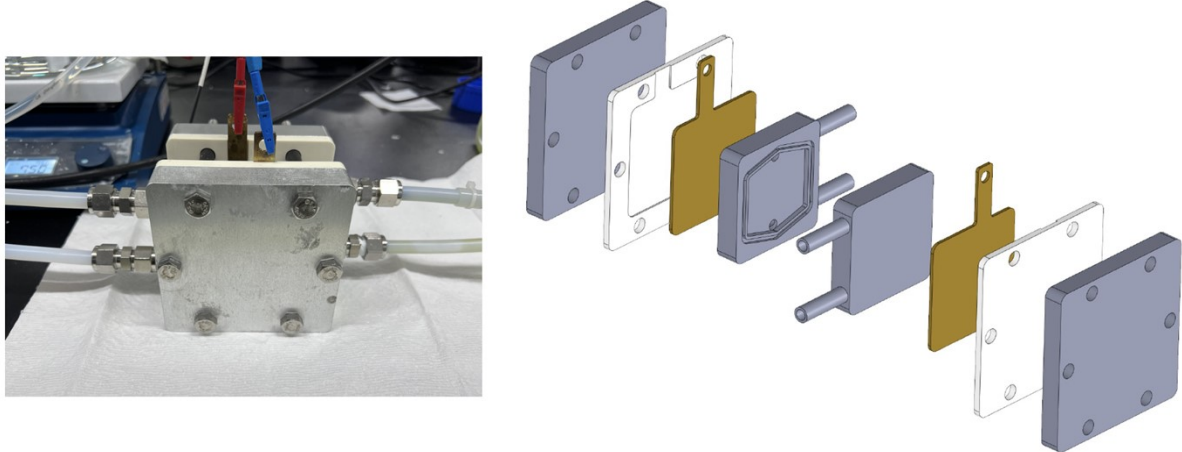


Figure S17. Flow electrolyzer setup. (Left) Photograph of the assembled flow electrolyzer used for coupled SOR-NO₃RR, showing inlet and outlet tubing connections and electrical wiring. (b) Exploded schematic diagram illustrating the components of the flow electrolyzer, including end plates, current collector, and flow channels.

Table S1. Summary of elemental composition analysis of MOF-derived CoS_x using Energy Dispersive X-ray Spectroscopy (EDX) at 50,000× magnification.

Label	at%				Total
	O	S	Co		
MOF derived CoS area 1 50000x 1	41.49	32.5	26.01		100
MOF derived CoS area 1 50000x 2	44.21	31.09	24.7		100
MOF derived CoS area 1 50000x 3	37.52	30.19	32.29		100
MOF derived CoS area 1 50000x 4	41.18	34.18	24.64		100
MOF derived CoS area 1 50000x 5	40.7	34.03	25.27		100
MOF derived CoS area 1 50000x 6	42.48	31.16	26.36		100

Table S2. Performance of the state-of-the-art SOR catalysts.

Material	Electrolytes	Potential at. j (V@mA cm ⁻²)	Duration of stability (h@mA cm ⁻² or V)	Cell voltage (V@mA cm ⁻²)	Ref.
MOF-derived CoS_x	1.0 M Na₂S + 1.0 M NaOH	0.46 V @50 mA cm⁻²	150 h@0.8 V	0.57 V@10 mA cm⁻² (SOR-NO₃RR)	This work
CoNi ₂ S ₄ NFs	1.0 M Na ₂ S + 1.0 M NaOH	0.53 V @50 mA cm ⁻²	20 h@10 mA cm ⁻²	0.3 V@10 mA cm ⁻²	[1]
WS ₂ NNs	1.0 M Na ₂ S + 1.0 M NaOH	0.6 V @57.60 mA cm ⁻²	192 h@1.3 V	1.17 V@10 mA cm ⁻²	[2]
Vpd·Pd ₄ SMNRs	4.0 M Na ₂ S + 1.0 M NaOH	0.65 V @100mA cm ⁻²	120 h@0.5 V	0.77 V @100 mA cm ⁻²	[3]
Fe ₃ C@N-CNTs/IF	1.0 M Na ₂ S + 1.0 M NaOH	0.46 V @10mA cm ⁻²	/	0.99 V@10 mA cm ⁻² (SOR-NO ₃ RR)	[4]
CoNi@NGs	1.0 M Na ₂ S + 1.0 M NaOH	0.52 V @100mA cm ⁻²	500 h@30 mA cm ⁻²	/	[5]
SnSe ₂	1.0 M Na ₂ S + 1.0 M NaOH	0.42 V @10 mA cm ⁻²	18 h@10 mA cm ⁻²	/	[6]
Co-Ni ₃ S ₂	1.0 M Na ₂ S + 1.0 M NaOH	0.59 V @100 mA cm ⁻²	24 h@50 mA cm ⁻²	0.80 V@50 mA cm ⁻²	[7]
CuCoS/CC	4.0 M Na ₂ S + 1.0 M NaOH	1.33 V @100 mA cm ⁻²	20 h@10 mA cm ⁻²	0.75 V@100 mA cm ⁻²	[8]
HEDP-Rh metallene	4.0 M Na ₂ S + 1.0 M NaOH	0.538 V @100 mA cm ⁻²	125 h@0.8 V	1 V@100 mA cm ⁻²	[9]
Fe, F-NiO	1.0 M Na ₂ S 1.0 M KOH	0.63 V @100 mA cm ⁻²	100 h@1.74 V	/	[10]
SP-Rhlene	4.0 M Na ₂ S + 1.0 M KOH	0.38 V @10 mA cm ⁻²	120 h@0.8 V	0.385 V@10 mA cm ⁻²	[11]
MFe ₂ O ₄	1.0 M Na ₂ S + 1.0 M NaOH	0.45 V @10 mA cm ⁻²	25 h@10 mA cm ⁻²	1.14 V@10 mA cm ⁻² (SOR-NO ₃ RR)	[12]

Table S3. Performance of the state-of-the-art NO₃RR catalysts.

Material	Electrolytes	Highest FE (%)	NH ₃ yield rate (mg h ⁻¹ cm ⁻²)	Ref.
MOF-derived CoS_x	0.1 M NaNO₃ + 1.0 M NaOH	93.4	9.1	This work
BCN@Ni	0.1 M KNO ₃ + 0.1 M KOH	91.1	2.3	[13]
RM (Fe ₂ O ₃ +Al _x Si _y O)	1.0 M KNO ₃ + 1.0 M PBS	92.8	2.7	[14]
Fe ₃ O ₄ /SS	0.1 M NaNO ₃ + 0.1 M NaOH	91.5	10.1	[15]
Fe SAC	0.5 M KNO ₃ + 0.1 M K ₂ SO ₄	75	7.8	[16]
PTCDA/O-Cu	500 ppm NaNO ₃ + 0.1 M PBS	77	0.43	[17]
Cu-N-C	0.1 M KNO ₃ + 0.1 M KOH	84.7	4.5	[18]
Co-Fe@Fe ₂ O ₃	1000 ppm NaNO ₃ + 0.1M Na ₂ SO ₄	85.8	1.5	[19]
Cu@C	1.0 mM NaNO ₃ + 1.0 M KOH	72	0.47	[20]
Co NPs@C	0.05 M NaNO ₃ + 0.2 M NaHCO ₃	54.3	2.21	[21]
Ir NTs	1.0 M NaNO ₃ + 0.1 M HClO ₄	84.7	0.92	[22]
Cu ₂ O+Cu ₃ O ₄	0.1 M NaNO ₃ + 0.1 M NaOH	85.4	12.76	[23]
Cu@NF	200 ppm KNO ₃ -N + 1 M KOH	96.6	4.28	[24]

References

- [1] H. Wang, B. Wang, H. Yu, K. Deng, Y. Xu, X. Li, Z. Wang, L. Wang, Bifunctional Cobalt–Nickel Sulfide Nanoflowers as Electrocatalysts for Concurrent Energy-Efficient Hydrogen Production and Sulfur Recycling, *ACS Applied Nano Materials* 6(12) (2023) 10863-10871. <https://doi.org/10.1021/acsanm.3c02247>.
- [2] L. Yi, Y. Ji, P. Shao, J. Chen, J. Li, H. Li, K. Chen, X. Peng, Z. Wen, Scalable Synthesis of Tungsten Disulfide Nanosheets for Alkali-Acid Electrocatalytic Sulfion Recycling and H₂ Generation, *Angewandte Chemie International Edition* 60(39) (2021) 21550-21557. <https://doi.org/https://doi.org/10.1002/anie.202108992>.
- [3] W. Wang, Q. Mao, S. Jiang, K. Deng, H. Yu, Z. Wang, Y. Xu, L. Wang, H. Wang, Heterophase Pd₄S metallene nanoribbons with Pd-rich vacancies for sulfur ion degradation-assisted hydrogen production, *Applied Catalysis B: Environmental* 340 (2024) 123194. <https://doi.org/https://doi.org/10.1016/j.apcatb.2023.123194>.
- [4] W. Yu, J. Yu, Y. Wang, X. Li, Y. Wang, H. Yuan, X. Zhang, H. Liu, W. Zhou, Electrocatalytic upcycling of nitrate and hydrogen sulfide via a nitrogen-doped carbon nanotubes encapsulated iron carbide electrode, *Applied Catalysis B: Environmental* 310 (2022) 121291. <https://doi.org/https://doi.org/10.1016/j.apcatb.2022.121291>.
- [5] M. Zhang, J. Guan, Y. Tu, S. Chen, Y. Wang, S. Wang, L. Yu, C. Ma, D. Deng, X. Bao, Highly efficient H₂ production from H₂S via a robust graphene-encapsulated metal catalyst, *Energy & Environmental Science* 13(1) (2020) 119-126. <https://doi.org/10.1039/C9EE03231B>.
- [6] W. Feng, M. Cheng, R. Du, Y. Wang, P. Wang, H. Li, L. Song, X. Wen, J. Yang, X. Li, J. He, J. Shi, Gram-Scale Synthesized Two-Dimensional VSe₂ and SnSe₂ for Ultrahigh Electrocatalytic Sulfion Recycling, *Advanced Materials Interfaces* 9(13) (2022) 2200060. <https://doi.org/https://doi.org/10.1002/admi.202200060>.
- [7] Y. Li, Y. Duan, K. Zhang, W. Yu, Efficient anodic chemical conversion to boost hydrogen evolution with low energy consumption over cobalt-doped nickel sulfide electrocatalyst, *Chemical Engineering Journal* 433 (2022) 134472. <https://doi.org/https://doi.org/10.1016/j.cej.2021.134472>.
- [8] H. Yu, W. Wang, Q. Mao, K. Deng, Y. Xu, Z. Wang, X. Li, H. Wang, L. Wang, Electrocatalytic sulfion recycling assisted energy-saving hydrogen production using CuCo-based nanosheet arrays, *Journal of Materials Chemistry A* 11(5) (2023) 2218-2224. <https://doi.org/10.1039/D2TA08730H>.
- [9] Z. Wang, G. Yang, P. Tian, X. Li, K. Deng, H. Yu, Y. Xu, H. Wang, L. Wang, Hydrophilic functionalization of rhodium metallene for saving-energy hydrogen production and sulfur recovery, *Chemical Engineering Journal* 473 (2023) 145147. <https://doi.org/https://doi.org/10.1016/j.cej.2023.145147>.
- [10] C. Lyu, Y. Li, J. Cheng, Y. Yang, K. Wu, J. Wu, H. Wang, W.-M. Lau, Z. Tian, N. Wang, J. Zheng, Dual Atoms (Fe, F) Co-Doping Inducing Electronic Structure Modulation of NiO Hollow Flower-Spheres for Enhanced Oxygen Evolution/Sulfion Oxidation Reaction Performance, *Small* 19(38) (2023) 2302055. <https://doi.org/https://doi.org/10.1002/smll.202302055>.
- [11] H. Wang, Y. Liang, S. Liu, X. Mu, H. Yu, K. Deng, Z. Wang, Y. Xu, L. Wang, Electronic and active site engineering in Rh metallene via phosphorus and sulfur dual-doping for electrocatalytic sulfion recycling and hydrogen generation, *Inorganic Chemistry Frontiers* 10(19) (2023) 5686-5693. <https://doi.org/10.1039/D3QI00994G>.
- [12] J. Ding, L. Zhang, Z. Wei, Z. Wang, Q. Liu, G. Hu, J. Luo, X. Liu, Coupling Nitrate-to-Ammonia Conversion and Sulfion Oxidation Reaction Over Hierarchical Porous Spinel MFe₂O₄

(M=Ni, Co, Fe, Mn) in Wastewater, Small 21(7) (2025) 2411317.
<https://doi.org/https://doi.org/10.1002/smll.202411317>.

- [13] X. Zhao, Z. Zhu, Y. He, H. Zhang, X. Zhou, W. Hu, M. Li, S. Zhang, Y. Dong, X. Hu, A.V. Kuklin, G.V. Baryshnikov, H. Ågren, T. Wågberg, G. Hu, Simultaneous anchoring of Ni nanoparticles and single-atom Ni on BCN matrix promotes efficient conversion of nitrate in water into high-value-added ammonia, Chemical Engineering Journal 433 (2022) 133190.
<https://doi.org/https://doi.org/10.1016/j.cej.2021.133190>.
- [14] Y.-T. Xu, K.-C. Ren, Z.-M. Tao, D.K. Sam, E. Feng, X. Wang, G. Zhang, J. Wu, Y. Cao, A new catalyst based on disposed red mud for the efficient electrochemical reduction of nitrate-to-ammonia, Green Chemistry 25(2) (2023) 589-595. <https://doi.org/10.1039/D2GC02527B>.
- [15] X. Fan, L. Xie, J. Liang, Y. Ren, L. Zhang, L. Yue, T. Li, Y. Luo, N. Li, B. Tang, Y. Liu, S. Gao, A.A. Alshehri, Q. Liu, Q. Kong, X. Sun, In situ grown Fe₃O₄ particle on stainless steel: A highly efficient electrocatalyst for nitrate reduction to ammonia, Nano Research 15(4) (2022) 3050-3055. <https://doi.org/10.1007/s12274-021-3951-5>.
- [16] Z.-Y. Wu, M. Karamad, X. Yong, Q. Huang, D.A. Cullen, P. Zhu, C. Xia, Q. Xiao, M. Shakouri, F.-Y. Chen, J.Y. Kim, Y. Xia, K. Heck, Y. Hu, M.S. Wong, Q. Li, I. Gates, S. Siahrostami, H. Wang, Electrochemical ammonia synthesis via nitrate reduction on Fe single atom catalyst, Nature Communications 12(1) (2021) 2870. <https://doi.org/10.1038/s41467-021-23115-x>.
- [17] G.-F. Chen, Y. Yuan, H. Jiang, S.-Y. Ren, L.-X. Ding, L. Ma, T. Wu, J. Lu, H. Wang, Electrochemical reduction of nitrate to ammonia via direct eight-electron transfer using a copper-molecular solid catalyst, Nature Energy 5(8) (2020) 605-613. <https://doi.org/10.1038/s41560-020-0654-1>.
- [18] J. Yang, H. Qi, A. Li, X. Liu, X. Yang, S. Zhang, Q. Zhao, Q. Jiang, Y. Su, L. Zhang, J.-F. Li, Z.-Q. Tian, W. Liu, A. Wang, T. Zhang, Potential-Driven Restructuring of Cu Single Atoms to Nanoparticles for Boosting the Electrochemical Reduction of Nitrate to Ammonia, Journal of the American Chemical Society 144(27) (2022) 12062-12071. <https://doi.org/10.1021/jacs.2c02262>.
- [19] S. Zhang, M. Li, J. Li, Q. Song, X. Liu, High-ammonia selective metal-–organic framework-–derived Co-doped Fe/Fe₂O₃ catalysts for electrochemical nitrate reduction, Proceedings of the National Academy of Sciences 119(6) (2022) e2115504119. <https://doi.org/doi:10.1073/pnas.2115504119>.
- [20] Z. Song, Y. Liu, Y. Zhong, Q. Guo, J. Zeng, Z. Geng, Efficient Electroreduction of Nitrate into Ammonia at Ultralow Concentrations Via an Enrichment Effect, Advanced Materials 34(36) (2022) 2204306. <https://doi.org/https://doi.org/10.1002/adma.202204306>.
- [21] X. Fan, C. Liu, X. He, Z. Li, L. Yue, W. Zhao, J. Li, Y. Wang, T. Li, Y. Luo, D. Zheng, S. Sun, Q. Liu, L. Li, W. Chu, F. Gong, B. Tang, Y. Yao, X. Sun, Efficient Electrochemical Co-Reduction of Carbon Dioxide and Nitrate to Urea with High Faradaic Efficiency on Cobalt-Based Dual-Sites, Advanced Materials 36(25) (2024) 2401221. <https://doi.org/https://doi.org/10.1002/adma.202401221>.
- [22] J.-Y. Zhu, Q. Xue, Y.-Y. Xue, Y. Ding, F.-M. Li, P. Jin, P. Chen, Y. Chen, Iridium Nanotubes as Bifunctional Electrocatalysts for Oxygen Evolution and Nitrate Reduction Reactions, ACS Applied Materials & Interfaces 12(12) (2020) 14064-14070. <https://doi.org/10.1021/acsmami.0c01937>.
- [23] J. Zhang, W. He, T. Quast, J.R.C. Junqueira, S. Saddeler, S. Schulz, W. Schuhmann, Single-entity Electrochemistry Unveils Dynamic Transformation during Tandem Catalysis of Cu₂O and

Co₃O₄ for Converting NO₃⁻ to NH₃, Angewandte Chemie International Edition 62(8) (2023) e202214830. <https://doi.org/https://doi.org/10.1002/anie.202214830>.

[24] J. Li, J. Gao, T. Feng, H. Zhang, D. Liu, C. Zhang, S. Huang, C. Wang, F. Du, C. Li, C. Guo, Effect of supporting matrixes on performance of copper catalysts in electrochemical nitrate reduction to ammonia, Journal of Power Sources 511 (2021) 230463. <https://doi.org/https://doi.org/10.1016/j.jpowsour.2021.230463>.